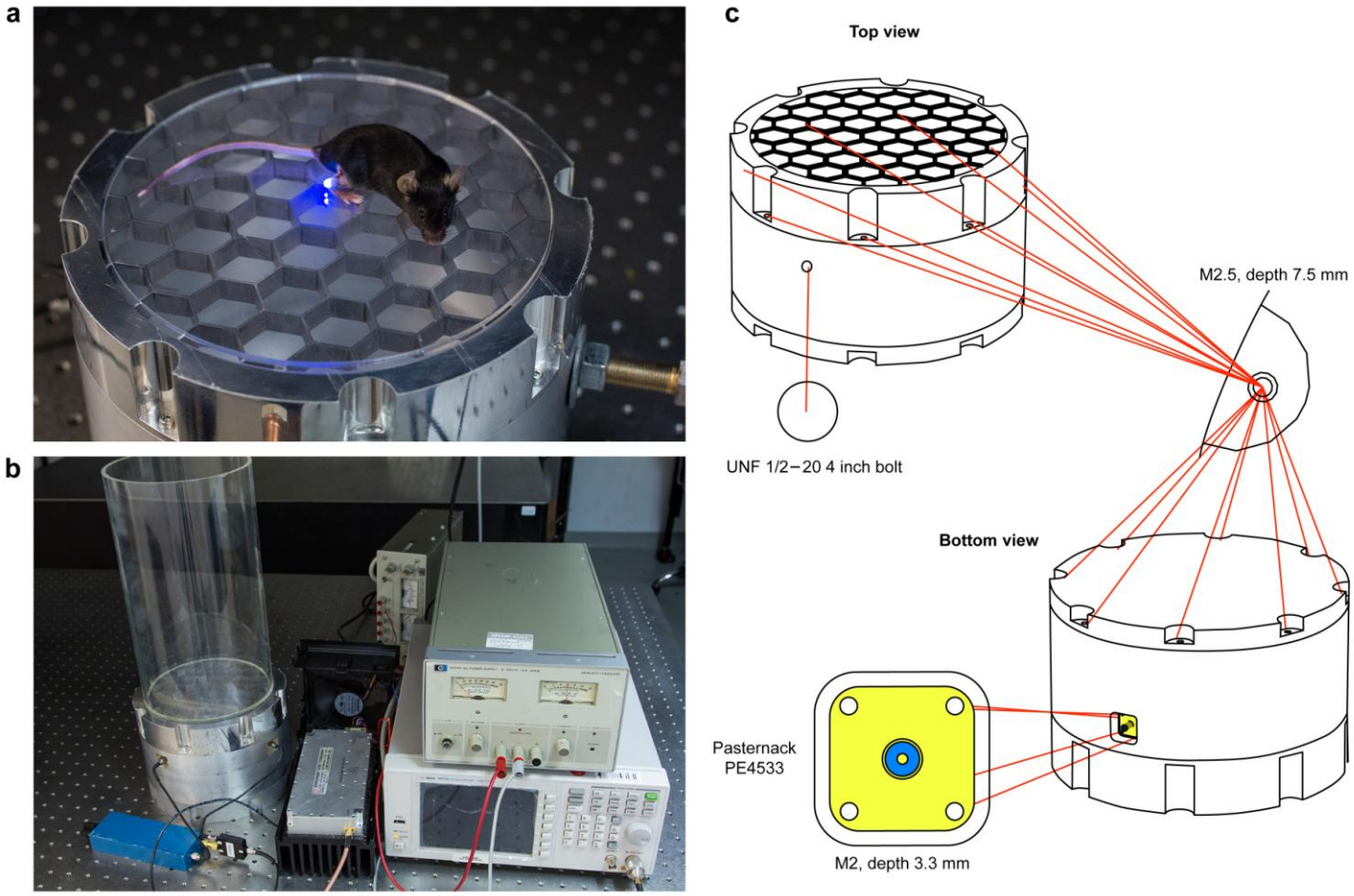

Supplementary Figure 1

Resonant cavity and power source.

(a) Resonant cavity powers a wireless device in a mouse on the surface of the cavity. (b) Total setup: the mouse enclosure above the resonant cavity, resonant cavity, phase shifter, signal generator, amplifier, and fan. (c) Drawing for use with assembling the components (**Supplementary Data**) of the cavity.

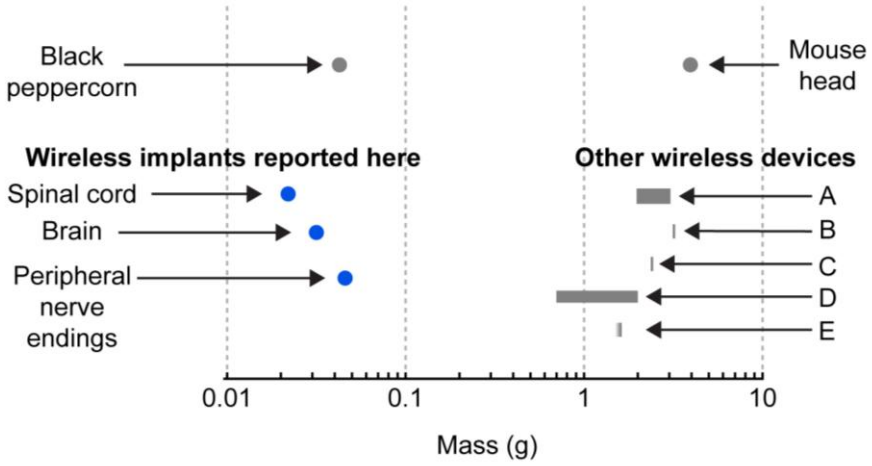

Supplementary Figure 2

Size comparison of fully internal wireless implants.

Devices reported here have the same approximate mass of a black peppercorn and are much smaller than previously reported wireless optogenetic systems (A–E); reported ranges of mass represented by rectangles. A: Wentz, C.T., et al. A wirelessly powered and controlled device for optical neural control of freely-behaving animals. *J Neural Eng* **8**, 046021 (2011). B: Iwai, Y., Honda, S., Ozeki, H., Hashimoto, M. & Hirase, H. A simple head-mountable LED device for chronic stimulation of optogenetic molecules in freely moving mice. *Neurosci Res* **70**, 124–127 (2011). C: Hashimoto, M., Hata, A., Miyata, T. & Hirase, H. Programmable wireless light-emitting diode stimulator for chronic stimulation of optogenetic molecules in freely moving mice. *Neurophotonics* **1**, 011002 (2014). D: Kim, T.I., et al. Injectable, cellular-scale optoelectronics with applications for wireless optogenetics. *Science* **340**, 211–216 (2013). E: Lee, S., et al. A miniature, fiber-coupled, wireless, deep-brain optogenetic stimulator. *IEEE Trans Neural Syst Rehabil Eng* (2015).

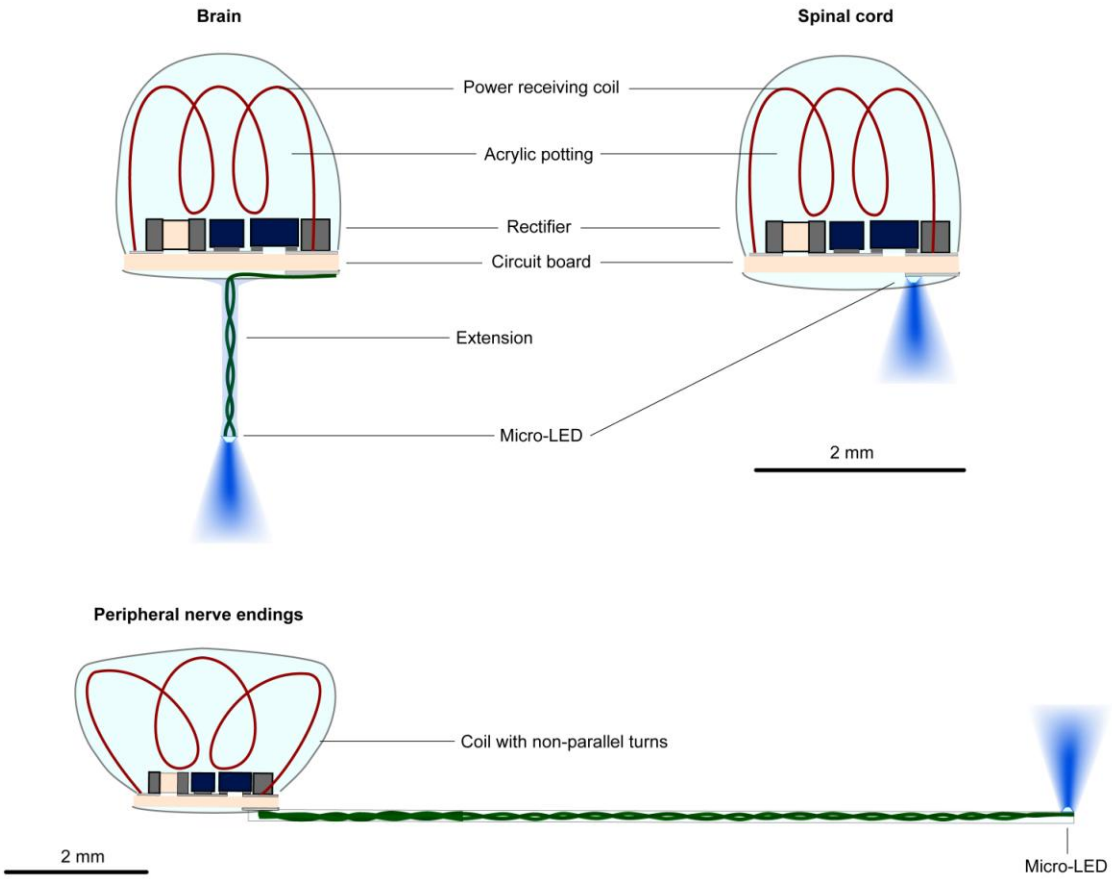

Supplementary Figure 3

Wireless implants for the brain, spinal cord and peripheral nerve endings.

Similar construction is used for all implants, but small design variations are used to customize the implants to different nervous system targets. In brain and peripheral implants, current is delivered to a 250-μm diameter extension made of a pair of magnet wires with a micro-LED attached at the tip. The extension can be inserted in the brain or routed to peripheral nerves. The micro-LED of the brain implant points parallel to the extension axis, whereas that of the peripheral nerve ending implant points perpendicular to the extension axis. Such an extension was not included in the spinal implant to avoid damage to the cord; instead, the LED was mounted directly onto the PCB. A “spinal cord” device could equivalently be used for superficial brain targets. Peripheral implants change spatial orientation relative to the cavity more than central implants during the course of locomotion. Due to this variability in orientation of the peripheral implant, the individual turns of the coil were set to be non-parallel, thus minimizing orientation-related power fluctuations.

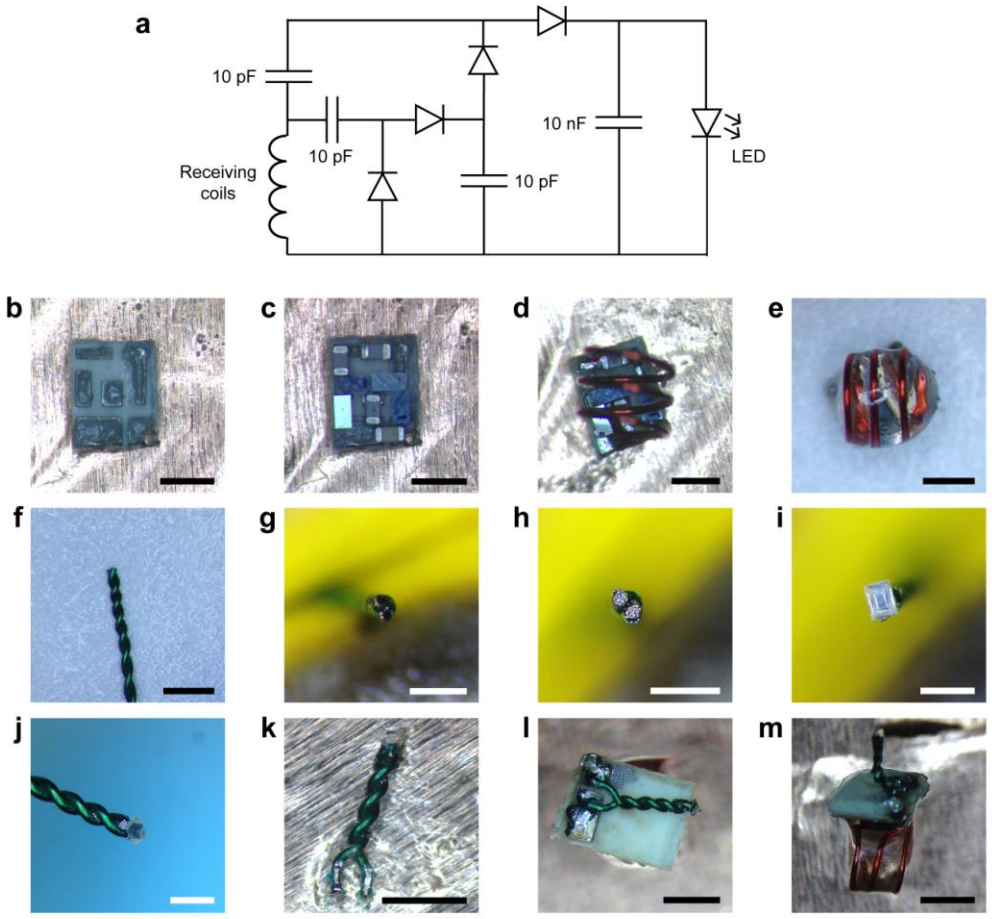

Supplementary Figure 4

Step-by-step construction of implants.

(a) Circuit diagram of the rectifier. This circuit converts RF energy received from the implant coil to direct current for the LED. It is a two-stage voltage doubling circuit using Schottky diodes. (b) The printed circuit board (PCB) was cut to size, and solder paste was applied to the metal traces on the PCB. (c) The surface-mount devices (SMD) were bonded with reflow soldering. (d) The power receiving coil was soldered to the PCB. (e) The coil and SMD components were stabilized with acrylic. (f) The extension was formed from a pair of twisted 36 G wires. (g) The ends of the twisted wires were separated by 70 μm. (h) Solder paste was applied to the tips of the bared wires. (i) The LED was placed on the ends of the wires. (j) The extension was positioned for reflow with a butane torch (post-reflow not shown). (k) The extension was cut to desired length and tested for polarity. (l) The extension was soldered to the bottom of the PCB. (m) The extension was bent to the desired angle and a final coat of acrylic was applied. Scale bars: black, 1 mm; white, 0.5 mm.

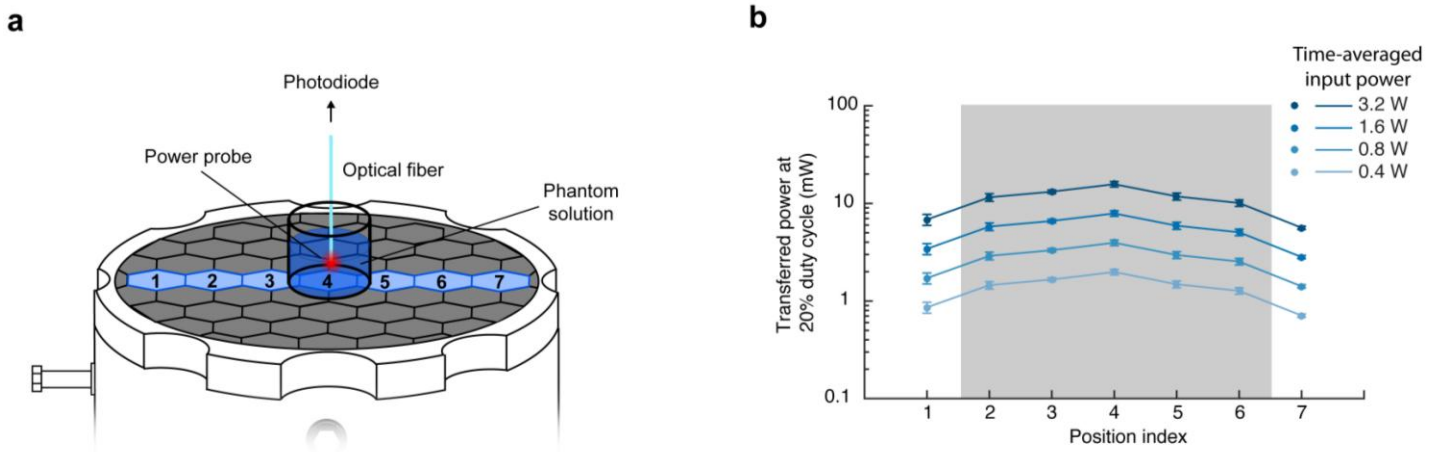

Supplementary Figure 5

Power transferred to the wireless implant at different positions and input power levels.

(a) Measurement probe consisting of an LED and the same coil and rectifier circuitry as the brain and spinal cord implants. Light from the LED is directed to a photodiode through a silica optical fiber. (b) Power transferred to the implant at the output of the rectifier circuitry as a function of input power and position on the resonant cavity. Typical operating region on the cavity surface is shaded. The implant is operated at a 20% duty cycle; instantaneous transferred power and time-averaged input power are shown (n = 4 technical trials at each location).

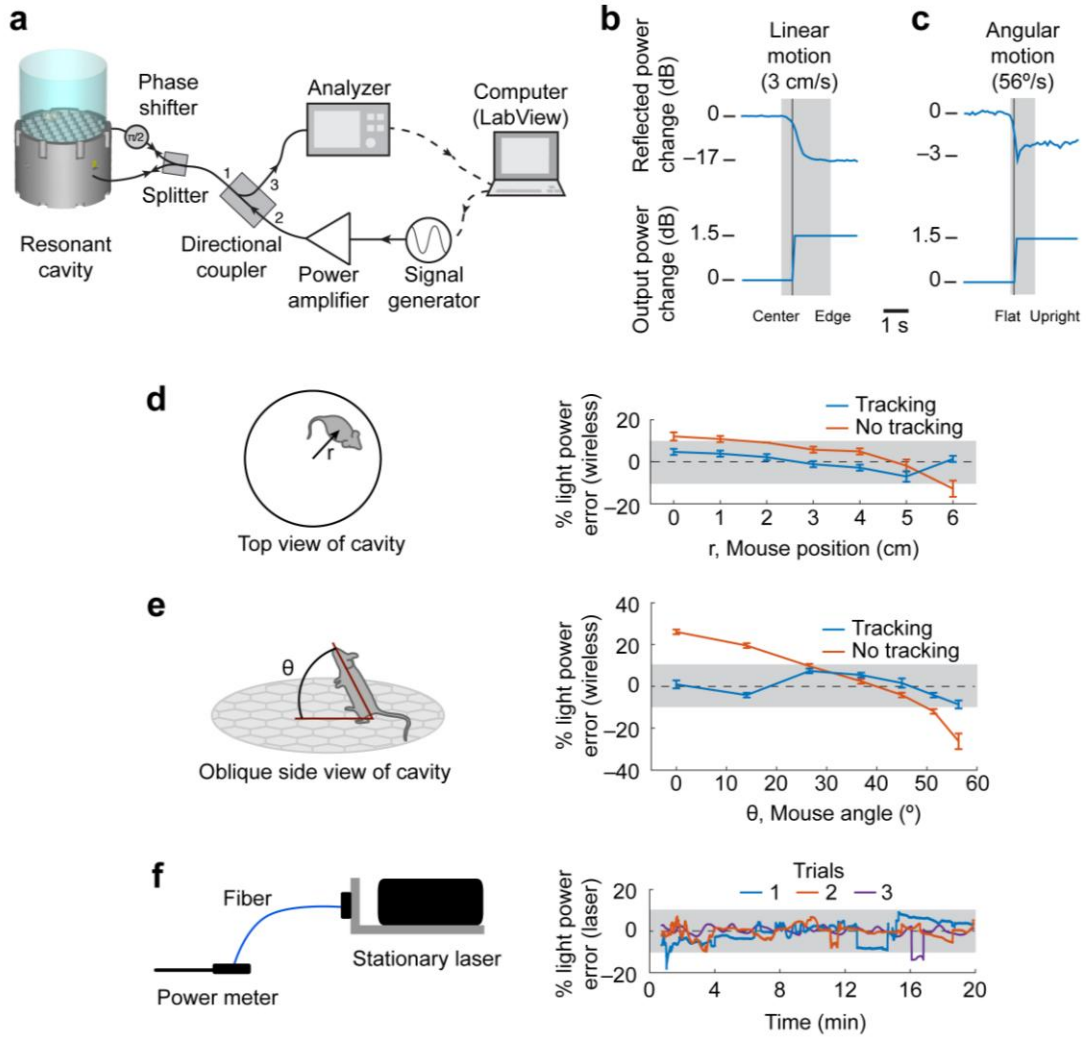

Supplementary Figure 6

Closed-loop reflection monitoring reduces variability in received power.

(a) Experimental setup describing system for closed-loop adjustment of delivered power based on measurements on reflected power (**Supplementary Note 1**). Solid lines: power flow; dashed lines: control signals. (b) Real-time tracking with linear motion: output power increases when reflected power decreases. c) Real-time tracking with angular motion: output power increases when reflected power decreases. (d-e) Closed loop monitoring reduces variability in delivered power with changes in mouse position (d), and mouse angle (e) to within ± 10%. Center values: means, error bars: S.E.M. (*n* = 3 technical replicates). (f) Measurements of 'normal' stochastic variation in laser output. Variation magnitude in commonly used laser systems is similar to that achieved with closed-loop wireless system.

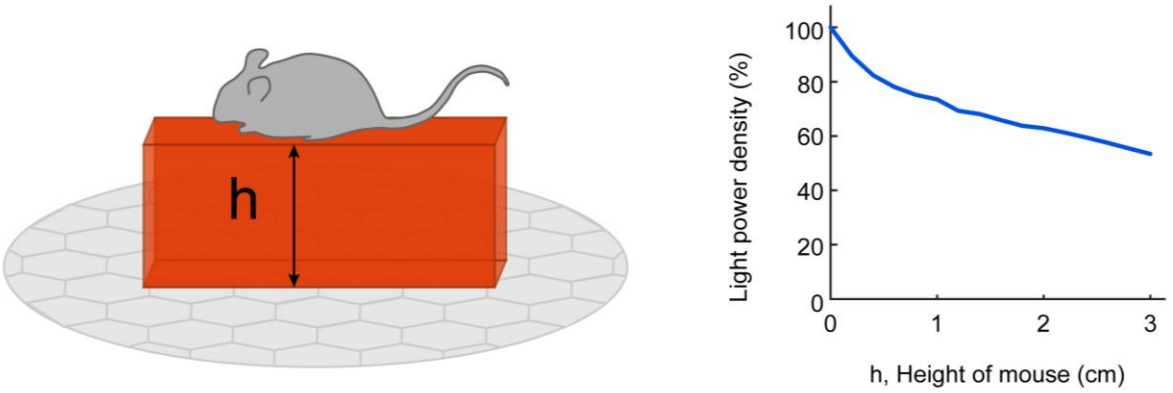

Supplementary Figure 7

Simulated power density as a function of the height, *h*, of the mouse above the surface of the cavity.

Thickness of the floor of the behavior chamber or bedding could alter height and therefore decrease delivered power, and should be accounted for (**Supplementary Note 2**).

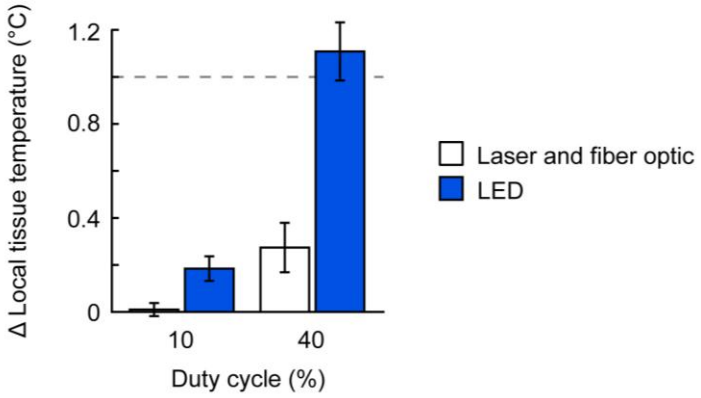

Supplementary Figure 8

Local heating due to LED compared to heating due to light from a fiber-coupled laser (20 mW/mm^2).

Local temperature of brain tissue of mice was measured with inserted probe (**Supplementary Note 3**). Center values: means, error bars: S.E.M. (*n* = 3 trials).

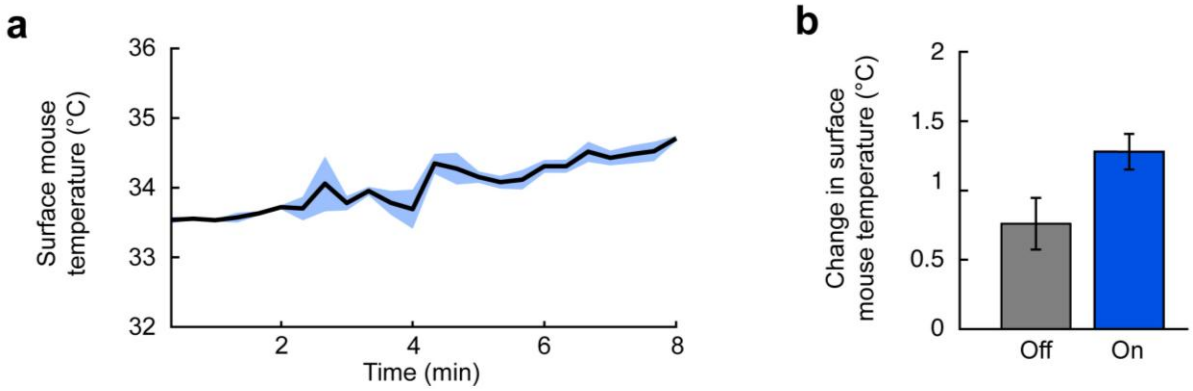

Supplementary Figure 9

Surface mouse temperature due to radio-frequency heating (4-W average input power).

(a) Temperatures of mice were measured with thermal imaging with either the cavity power off or on without an implant over 8 minutes (*n* = 3 mice). (b) Final reading values for both cavity power off and cavity power on. The mice exhibited a temperature rise of 0.76 °C with the power off, perhaps due to increased behavior in the enclosure tube. The temperature rise attributed to the radio-frequency energy alone is 0.52 °C.

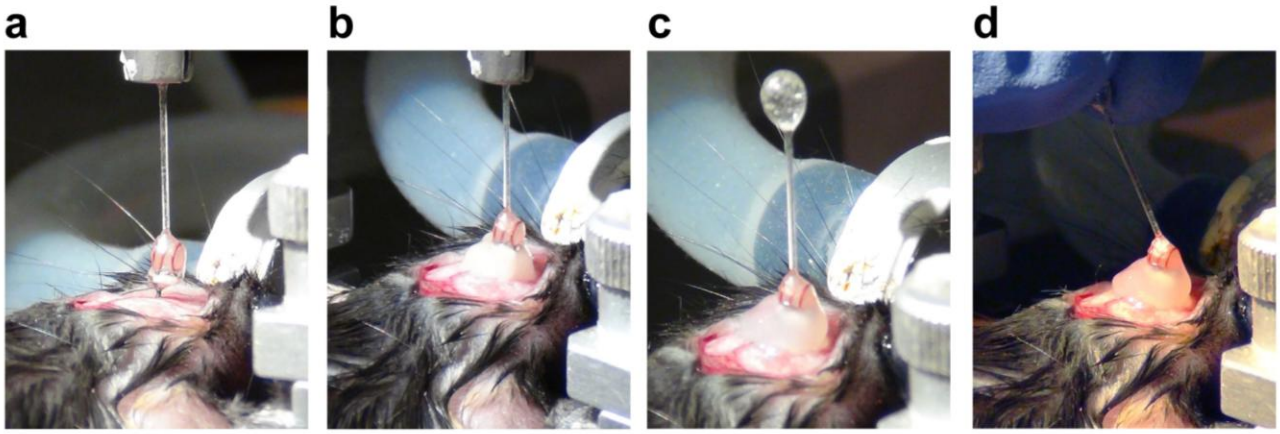

Supplementary Figure 10

Implantation of brain device to stimulate premotor cortex.

(a) Craniotomy is drilled in the skull and the implant is positioned at the specified x-y-z coordinates of the target brain structure, in this case just superior to M2 (AP: +1.0, ML: 0.5, DV: –0.5; see reference below) using the disposable glass implantation tool attached to the stereotactic positioner. (b) The implant is bonded in place using blue light curable composite (Pentron, N11WA). (c) The stereotactic positioner is unscrewed from the implantation tool and moved out of the way. (d) The implantation tool is gently twisted off, and the skin is then sutured over the implant. Reference: Franklin, K.B.J. & Paxinos, G. *The mouse brain in stereotaxic coordinates*, (Academic Press, San Diego, 1997).

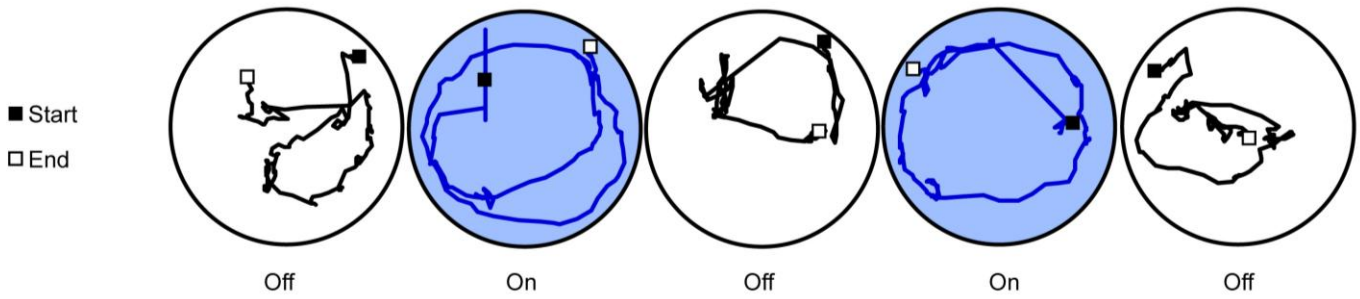

Supplementary Figure 11

Representative traces of mouse movement during on-off cycles (1 continuous session, 1 mouse).

Motor stimulation of the right motor cortex with 5 ms pulses at 20 Hz elicited circling behavior. Stimulation was wirelessly controlled in 20-s on-off cycles. Traces here representative of three out of five mice; the remaining two mice moved very little or not at all when cavity power was off.

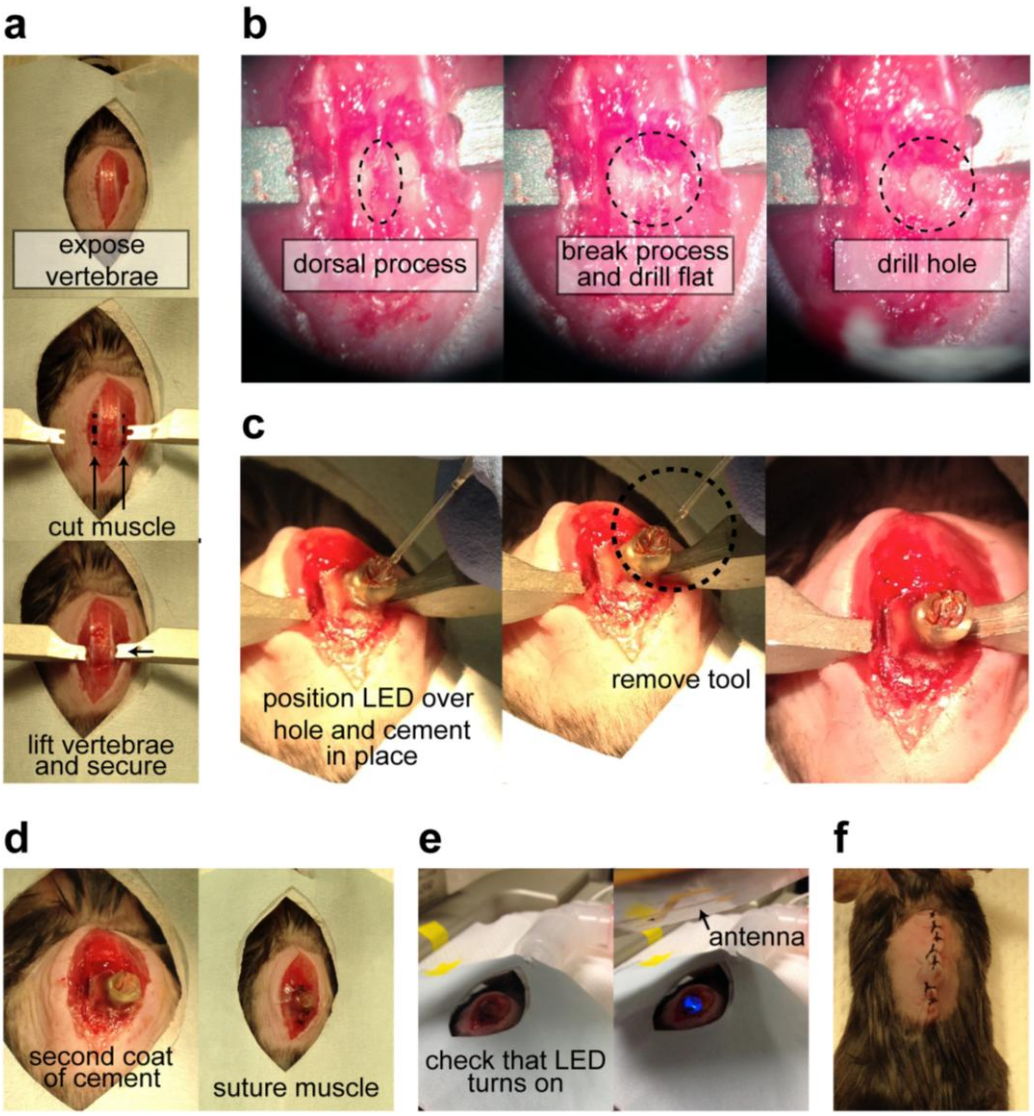

Supplementary Figure 12

Implantation of spinal cord device to stimulate superficial laminae of the dorsal spinal cord.

(a) The spinal column is exposed and secured in stereotactic adaptors for the spinal cord. (b) Superficial soft tissue is removed from the vertebrae. The dorsal process of the vertebra is broken off and then drilled flat. A hole is drilled into the now flat surface of the vertebra directly dorsal to the region to be stimulated. (c) LED is positioned over the hole in the vertebra, either by hand or with a stereotax, using the glass implantation tool. The implant is cemented in place, and the implantation tool is broken off. (d) A second coat of cement is applied before the muscle is sutured in place around the implant. (e) The implant is checked for functionality using an alternate antenna. (f) Skin is sutured over the implant.

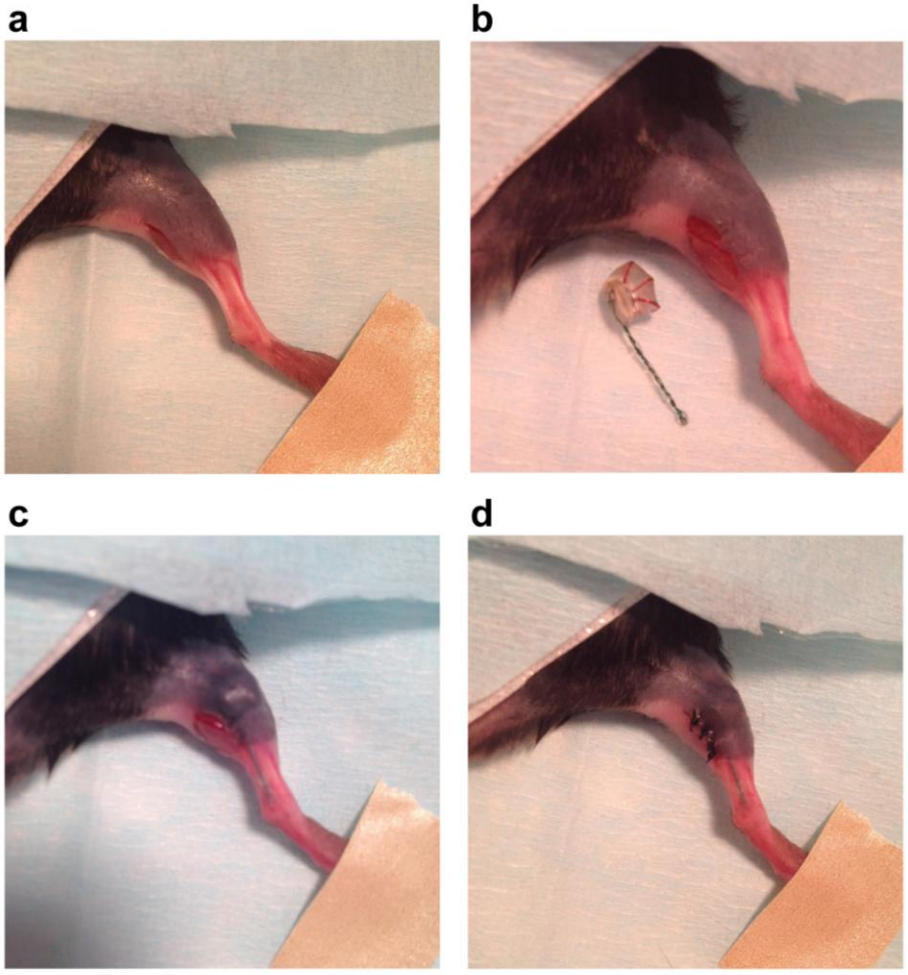

Supplementary Figure 13

Implantation of peripheral device to stimulate peripheral nerve endings in the heel of the mouse hind paw.

(a) Incision is made superficial to triceps surae muscles. (b) Size of implant compared to the incision. (c) LED at the tip of the extension is routed to the heel, and the power receiving coil is then placed under the skin, adjacent to the incision (not directly under it). (d) Incision is sutured.

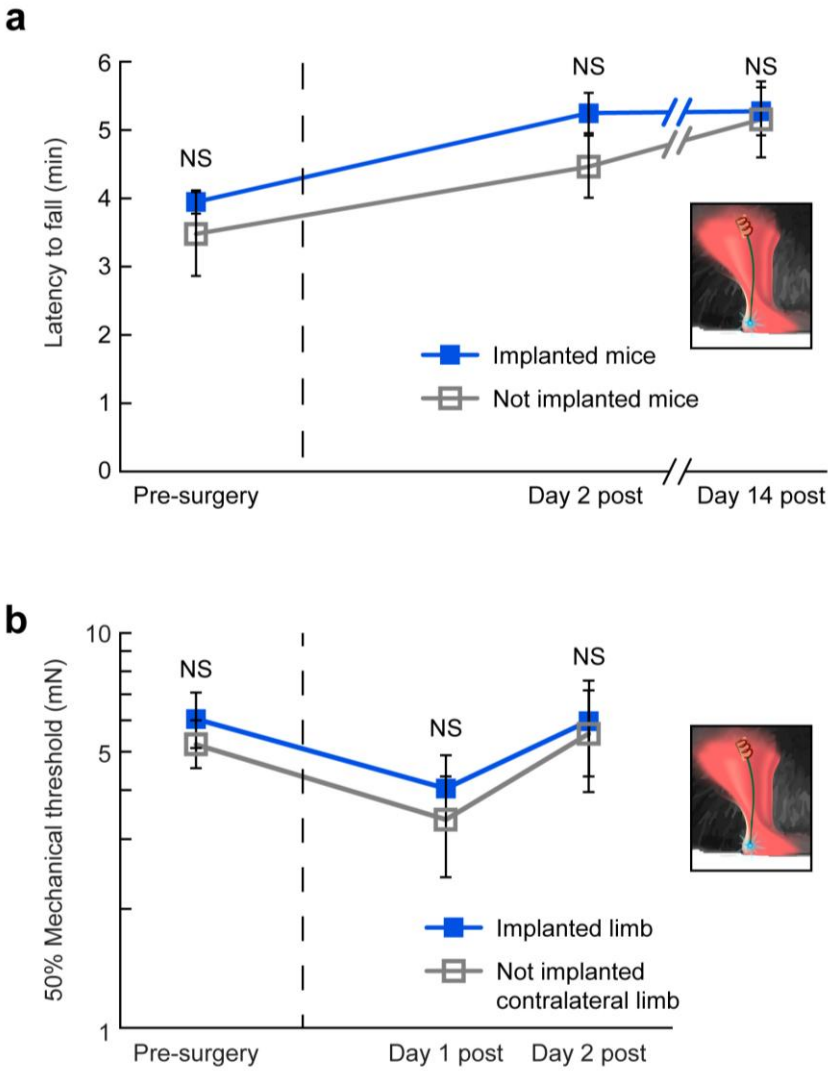

Supplementary Figure 14

Effect of implant alone on mobility and pain thresholds post-implantation.

LED was not powered on at any time. (a) Mice were evaluated for Rotarod performance before and after implantation of wireless device in lower hindlimb. Control mice did not undergo surgery. Rotarod latency was not significantly different between implanted and not implanted mice at any time point (n = 9 implanted mice, 10 not implanted mice, P [effect size (Hedge's g)] - Pre: 0.49 [0.31], Day two: 0.18 [0.62], Day fourteen: 0.86 [0.078]). (b) Mechanical (von Frey) threshold of mice before and after implantation of the wireless device in lower hind limb. Thresholds are not significantly different between the implanted limb and the contralateral limb at any time point (n = 9 mice, P [effect size (Hedge's g)] - Pre: 0.36 [0.30], Day one: 0.58 [0.23], Day two: 0.91 [0.0.085]).

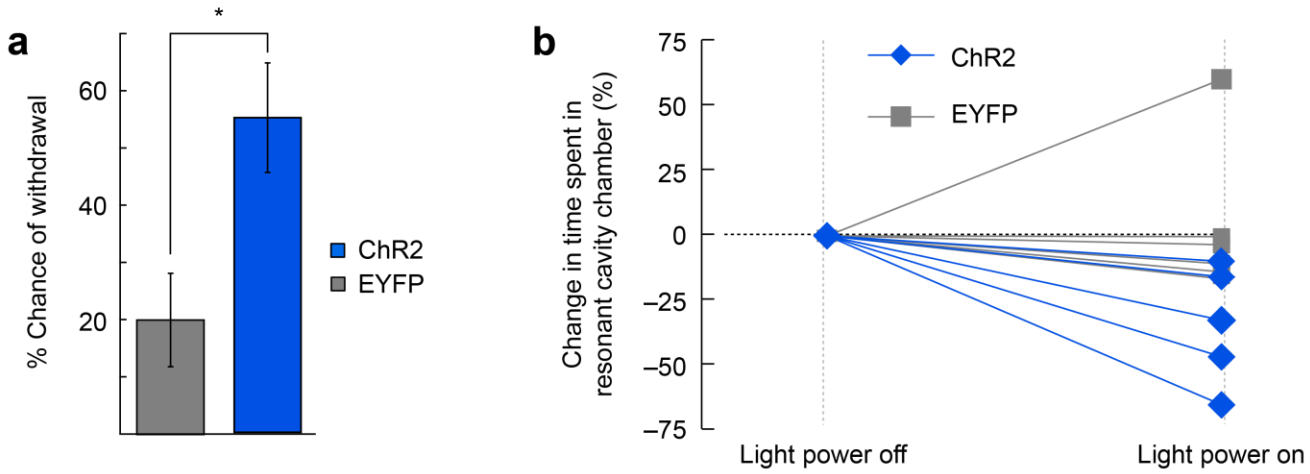

Supplementary Figure 15

Stimulation of peripheral nociceptors with a wireless device.

(a) Withdrawal latency test (cohort means): ChR2$^+$ mice withdrew their paws within a 20 s stimulation window significantly more often than EYFP$^+$ control mice (n = 4 ChR2$^+$ mice, 4 EYFP$^+$ mice, unpaired t-test, P = 0.03, effect size (Hedge's g) = 1.71). (b) Place aversion test (individual mice): All ChR2$^+$ mice implanted with the peripheral device spent less time in the resonant cavity chamber when the cavity was powered on (n = 5 ChR2$^+$ mice).

Supplementary Notes

Supplementary Note 1 | Improving consistency in light power density through closed loop measurement of reflected power. In the experiments described throughout this paper, we found consistency of achieved light power density to be adequate. For future experiments using this approach where greater consistency is required, we report a method to improve consistency through measurement of reflected power at the cavity ports. The measured reflected power is modulated by the instantaneous quality factor of the resonance, which is changed by mouse position on the surface of the cavity. Therefore, through measurement of reflected power, one can adjust the power delivered to the resonant cavity based on the reflected power to ensure consistent delivery of power to an implant.

We routed reflected power through a directional coupler (KTDC-C8025-30, Kete Microwave Electronics) and measured it using an analyzer (used here: E5072A, Agilent Technologies; a less expensive option: RF Power Meter, ImmersionRC). A computer then used this power signal to adjust the output power of the cavity via a custom LabView program (**Supplementary Data 2**). To empirically test this system, we placed a mouse cadaver within the cavity, and moved it around the cavity floor to simulate normal animal movement and rearing. The LabView program adjusted the power delivered to the cavity in real-time (**Supplementary Fig. 6a–e**). To compare this variability against currently used light-delivery systems, we measured light power variability in a fiber optic-coupled laser (laser: 465 nm, OEM Laser Systems; optical fiber: BFL37-300, Thorlabs; power meter: PM100, Thorlabs; **Supplementary Fig. 6f**). Each trial uses a different combination of laser and optical fiber (2 lasers, 2 optical fibers). Variation in emitted laser power was similarly ± 10%, with the caveat that laser power variation is stochastic, and does not depend on mouse position and rearing angle.

Supplementary Note 2 | Simulation to estimate variability in power capture as a function of vertical position. Power capture efficiency as a function of vertical position was reported in **Supplementary Figure 7**. The mouse was modeled as an ellipsoidal object about 5 cm along the major axis and 2.5 cm along the minor axis. We assume the material is homogenous muscle-like tissue, justified because the mouse dimensions are comparable to the wavelength in tissue so the mouse's interaction with fields are dominated by the averaged dielectric response. The mouse model was placed over the hexagonal lattice and an incident wave inserted along an infinite cylindrical waveguide beneath. The incident wave was circularly polarized so that the coupling was independent of the transverse (xy) orientation of the mouse. We performed simulations as the height was varied from 0–3 cm. The resonant cavity assumptions are less valid at vertical elevations greater than 3 cm, and we have therefore not reported simulated power transfer at vertical distances greater than 3 cm. We computed the energy stored in the tissue volume. This energy is then dissipated as heat or extracted by the implant. Since stored energy is averaged over the entire volume of the mouse, this simulation provides a good estimation of how power transfer efficiency varies.

Supplementary Note 3 | **Comparing laser- and LED-induced heating.** Because the heat production of lasers is managed remotely from the animal tissue, and because laser beams include a very narrow spectral spread, fiber optic delivery of light represents a best case scenario of heating for a given light power density. To measure the induced temperature change caused by the micro-LED probe compared to fiber optically-delivered laser light (300 μm core silica optical fiber; 465 nm, OEM Laser Systems, East Lansing MI), we used a fiber optic temperature measurement probe (Neoptix, T1 sensor, Reflex signal conditioner) to measure heating in deep brain structures for tissues directly adjacent to the micro-LED and tip of the fiber optic. The micro-LED probe, fiber optic, and optical fiber were attached together with adhesive tape and simultaneously inserted into the brain (AP: +1.1, ML: 1.5, DV: 4.2; see reference below) of an anesthetized mouse, using the surgical procedure as described in the Online Methods. We measured brain temperature for one minute prior to light delivery and two minutes during light delivery (sampling frequency: 1 Hz). To deliver light, current was driven through the LED or the laser was driven to produce a light power density of 20 mW/mm^2, with duty cycles of 5%, 10%, 20%, and 40% (5 ms pulse width; 10 Hz, 20Hz, 40 Hz, and 80 Hz frequencies, respectively, *n* = 3 trials). **Supplementary Figure 8** displays the average of the final 30 s of light delivery for each trial. Reference: Franklin, K.B.J. & Paxinos, G. *The mouse brain in stereotaxic coordinates*, (Academic Press, San Diego, 1997).

Supplementary Note 4 | **Measurement of motor performance and mechanical thresholds post-implantation of peripheral device.** Mice implanted with devices for peripheral nerve endings (**Fig. 5a** and **Supplementary Fig. 3**) were evaluated for locomotion and pain changes due to the presence of the implant without light stimulation (**Supplementary Fig. 14**). We measured latency to fall during a 4–40 rotations per minute (rpm) ramp over five minutes (0.12 rpm/s) in both implanted and non-implanted mice with a Rotarod apparatus (San Diego Instruments, Inc.) before surgery, 2 days after surgery, and 14 days after surgery. Two trials were collected per mouse per day, and the mean latency to fall was calculated for each mouse. Mice were habituated to the setup and trained at least one day prior to the first test (15 minutes habituation; 16 rpm for 2 minutes; 15 minutes rest; 16 rpm for 2 minutes). Animals were also trained at the beginning of each testing session with three practice trials (4–40 rpm ramp over 5 minutes). von Frey (Ugo Basile, 37450-277) was used to evaluate mechanical pain thresholds in both the implanted and contralateral limb using the up-and-down method (see reference below) before surgery, one day after surgery, and two days after surgery. The presence of the implant alone did not measurably influence sensorimotor performance as measured with Rotarod testing nor mechanical pain sensitivity as measured with von Frey. Reference: Chaplan, S.R., Bach, F.W., Pogrel, J.W., Chung, J.M. & Yaksh, T.L. Quantitative assessment of tactile allodynia in the rat paw. *J Neurosci Methods* **53**, 55–63 (1994).

Supplementary Note 5 | **Measurement of paw withdrawal.** Mice implanted with devices for peripheral nerve endings (**Fig. 5a** and **Supplementary Fig. 3**) were evaluated for acute paw withdrawal behavior when the device was turned on (10 Hz frequency, 10 ms pulse width, 10 mW/mm^2 light power density; 20 s trials, 5 trials per mouse). The percentage of trials in which each mouse rapidly withdrew its paw or displayed nocifensive behavior was reported (**Supplementary Fig. 15a**).

Supplementary Note 6 | **Equipment and settings.** Spinal cord sections were mounted and imaged using a Leica TCS SP5 confocal microscope. Images were gathered at room temperature with a 10× objective, or a 20× oil immersion objective (image resolution: 1.321 pixels/µm (10×), 2.642 pixels/µm (20×), image bit depth: 8, excitation/emission settings: EYFP: 514 nm (excitation), 525 - 600 nm (emission), Cy5 (for c-Fos): 633 nm (excitation), 650-750 nm (emission)). Only single-colored display lookup tables (LUT) were used, which were linear and covered the full range of the data. When necessary, images were stitched together using Fiji's stitching plug-in.